euspen's 19th International Conference & Exhibition, Bilbao, ES, June 2019
www.euspen.eu

Task specific uncertainty in measurement of freeform optics

Todd Noste[1], Laura Hopper[1], Jimmie Miller[1], Chris Evans[1]

[1]*University of North Carolina at Charlotte*

tnoste@uncc.edu, cevans52@uncc.edu

Abstract
Freeform optics offer new design freedoms, allowing improved imaging performance, reduced system size, or some combination thereof. Design methods and fabrication techniques evolve rapidly. Independent part metrology lags.
Freeform optics fabrication at UNC Charlotte is supported by a variety of independent metrology platforms. This paper focusses on a Moore Nanotech 100UMM with two hydrostatic linear axes with nanometer resolution positioning and two air bearing rotary axes. The ISO Guide to the Expression of Uncertainty in Measurement (GUM) states that the result of a measurement is incomplete without a statement of the uncertainty. This paper discusses evaluation of uncertainty in measurements of freeform optics using the 100UMM.
A mathematical model was developed for the machine using rotation and translation matrices, statistical descriptions of probing errors, etc. Machine error motions are characterized, and the measurement data corrected. Uncertainties in the correction are then propagated through the machine model (in a Monte Carlo approach) to generate a population of surfaces that might reasonably represent the surface shape and specified measurands, leading to an evaluation of task specific uncertainty.
In this presentation, we will review the machine model, the machine tool metrology, and the evaluation of task specific uncertainties in the measurements of freeform optics used in a 3-mirror anastigmatic telescope. On-machine probe calibration and metrology "tool path" generation will be discussed.

Measuring instrument, Metrology, Ultra-precision, Uncertainty

1. Technical Approach

Freeform optics can be described as optics with no axis of symmetry. They may also include large slopes and a substantial departure from a sphere making them difficult to measure with 'traditional' metrology techniques. A method to measure the 250 mm freeform reflective optics for a three-mirror anastigmatic telescope with a maximum slope of 8.9 degrees and provide an uncertainty estimate will be discussed. The Moore Nanotech 100UMM will be used as a coordinate measuring machine. A mathematical machine model will provide measurement correction with Monte Carlo simulation to provide an estimate of the measurement uncertainty. The steps to measuring the optics are outlined below.

Approach for determining task specific uncertainty:

1. Derive mathematical machine model with machine errors and nominal carriage movements
2. Measure machine errors and estimate uncertainty of those measurements
3. Measure freeform, correct measurement using model and machine error measurements
4. Run Monte Carlo simulation to evaluate the uncertainty for each measurement point, hence in measurands describing the surface form.

2. Moore Nanotech 100UMM

The Moore Nanotech 100UMM is a 4 axis measuring machine with two hydrostatic linear axes and two air bearing rotary axes. The machine is surrounded by an environmentally controlled enclosure which holds the temperature of the machine, hydrostatic oil exiting the bearing and surrounding air to 20 +/- 0.1 deg. C to reduce thermal effects. Temperature is also monitored independent of the environmental control system.

The optical scales of the machine are read for the four carriage positions independently from the machine controller and concurrently with the measurement probe. This allows for a continuous measurement of the optic as the probe scans the surface, unaffected by machine following error. There is an uncertainty contribution due to the variation in data age between the probe reading and the scale readings. The carriage orientation and coordinate system can be found in Figure 1.

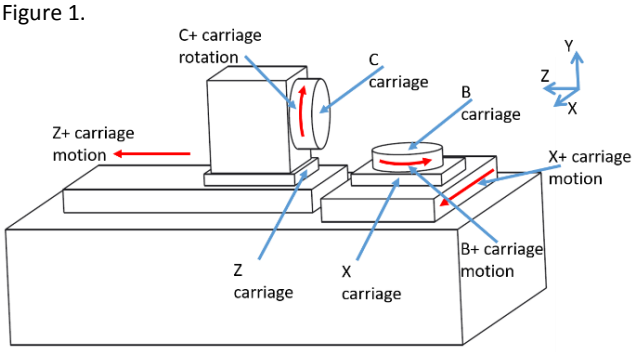

Figure 1. Showing the carriage orientation and directions of the Moore 100UMM.

The c carriage is associated with a rotation about the z axis and the b carriage around the y axis. The freeform optic being measured is mounted to the c carriage and the probe used is kinematically located in a 3-axis probe holder designed to enable probe position adjustment depending on specific measurement task. The probe holder is mounted on the b carriage.

2.1 On machine probe calibration

The probes used on the machine include: two chromatic confocal probes, linear variable differential transformer (LVDT) probe, capacitance linear variable displacement transducer (C-LVDT) probe, and capacitance gage providing contact and non-contact measurements. The probes are calibrated against the machine scales to correct for bias in the probes including non-linearity and for the analog probes establish the conversion to displacement. The uncertainty in these measurements will contribute to the combined uncertainty in the freeform optic measurements. A set of probe setting artifacts and procedures was developed to align the probe with the rotation axis of the c carriage. Additional procedures are being developed for determining the distance between the rotational axis of the b carriage and the measurement point of the probe for probe normal measurements.

3. Mathematical machine model

Using the naming convention in [1,2], the machine model is classified as a CZFXB where the c carriage supports the workpiece and the b carriage supports the probe. If we assign a coordinate system to each carriage and the frame, we can move between these coordinate systems with rotation and linear transformations which include the nominal movements as well as any errors associated with the motion. Starting from the frame, using a frame-based model, and working toward the measurement point there are two paths possible. One way is through the part and the other through the probe. These two paths can be set equal and solved for the measurement point in the c coordinate system.

3.1 Coordinate systems and fiducial origin

To define the coordinate systems, we make the origins overlap at a point called the fiducial origin defined at a nominal machine position where Z_0 is equal to Y_0 shown in Figure 2. The fiducial origin is also referred to as the functional point or point of interest. The machine errors will be measured with this origin in mind. To define the fiducial origin, it is assumed that the rotational axis of the c carriage is 'perfect' and will be used as the z axis of the frame coordinate system. A line perpendicular to the plane made by the rotational axis of the c carriage and the rotational axis of the b carriage will define the frame x axis. The frame y axis is simply perpendicular to both the x and z frame axes. It is assumed that the carriages, part, probe and frame are rigid bodies. The coordinate systems move in six degrees of freedom with their respective carriage.

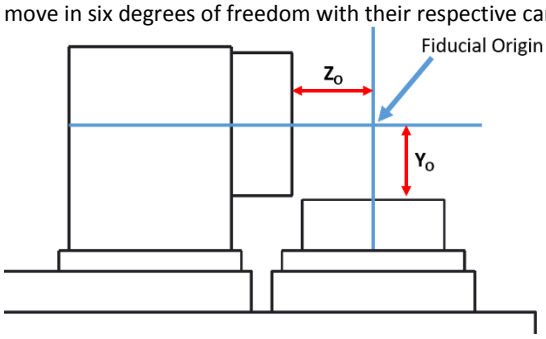

Figure 2. Showing the fiducial origin.

The fiducial origin is the point that the coordinate systems overlap and share orthogonal axes when Z_0 is equal to Y_0.

3.2 Error motions

For the four-carriage measuring machine, 32 errors will be considered. These errors are listed below in Table 1. The symbol $\delta_x(X)$ denotes the linear error in the "x" direction due to actuation of the "X" carriage. The symbol $\varepsilon_a(Z)$ is an angular error about the "x" axis due to actuation of the "Z" carriage. The nominal machine positions are designated by X for the x carriage, Z for the z carriage, β for the b carriage, and γ for the c carriage. The symbol $\alpha_{x.y}$ represents the squareness or parallelism error of the average motion of the "X" carriage origin about the "y" axis. There are eight possible squareness and parallelism errors, of which three will be unnecessary depending on how the coordinate systems are defined in the model and can be set to zero. It is important that the machine motion error metrology matches the model.

Table 1. Error notation based on [1].

Description	Errors
Linear displacement error in linear carriage	$\delta_x(X)$, $\delta_z(Z)$
Angular positioning error in rotary carriage	$\varepsilon_b(\beta)$, $\varepsilon_c(\gamma)$
Straightness errors	$\delta_y(X)$, $\delta_z(X)$,$\delta_x(Z)$, $\delta_y(Z)$, $\delta_x(\beta)$, $\delta_y(\beta)$,$\delta_z(\beta)$, $\delta_x(\gamma)$, $\delta_y(\gamma)$, $\delta_z(\gamma)$
Angular error – roll (around axis of movement)	$\varepsilon_a(X)$, $\varepsilon_c(Z)$
Angular error - pitch	$\varepsilon_c(X)$, $\varepsilon_a(Z)$
Angular error - yaw	$\varepsilon_b(X)$, $\varepsilon_b(Z)$
Angular errors in rotary carriages (tilt)	$\varepsilon_a(\beta)$, $\varepsilon_a(\gamma)$, $\varepsilon_b(\gamma)$, $\varepsilon_c(\beta)$
Squareness error between two axes / Parallelism	$\alpha_{x.y}$, $\alpha_{x.z}$, $\alpha_{z.x}$, $\alpha_{z.y}$, $\alpha_{b.x}$, $\alpha_{b.z}$, $\alpha_{c.x}$, $\alpha_{c.y}$

The errors are measured over the full travel of the carriage creating an error map as a function of carriage position to be used in the model. Since the errors are discrete measurements over the carriage position the need to interpolate between error measurement points is unavoidable.

The errors described above can be shown for a linear carriage and a rotary carriage with six possible errors for each. The six degrees of freedom of a rotary carriage includes the angular motions causing tilt in the carriage and a positioning error. The straightness measurements are the orthogonal deviations in the direction of the x, y, and z axes during the rotation of the carriage shown in Figure 3.

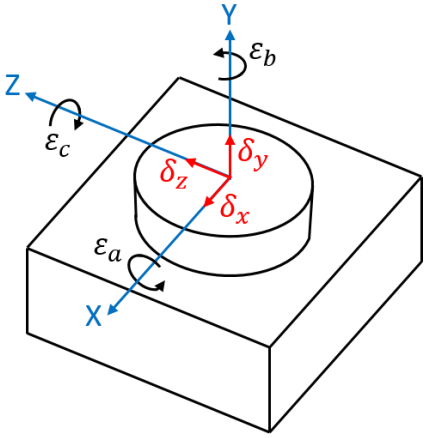

Figure 3. Showing the six error motions of a rotary carriage after [3].

The straightness errors in a linear carriage are a deviation of the origin of the carriage coordinate system perpendicular to the direction of motion or travel shown in Figure 4. The positioning error in the direction of travel is also a linear error. The angular errors are pitch, yaw and roll of the carriage during movement.

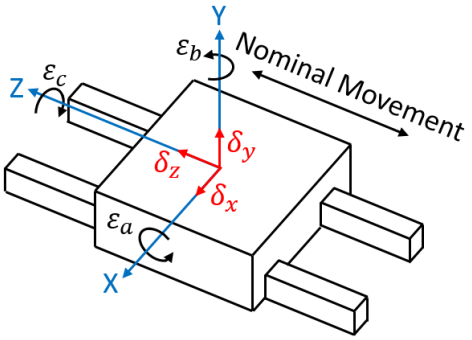

Figure 4. Showing the six error motions for a linear carriage after [3].

3.3 Building the model

To visualize the transformations between coordinate systems a diagram shown in Figure 5 is created showing the origin of each coordinate system, with ${}_{o}\mathrm{C}$ being the origin of the c coordinate system, and the vector between them. The vector changes as the carriages move in relation to each other.

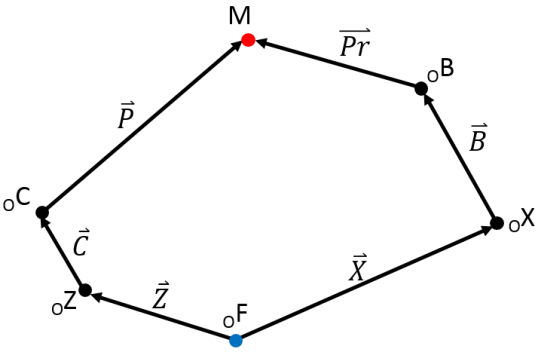

Figure 5. Frame based model with the coordinate systems and vectors between coordinate systems.

From Figure 5, the path to the measurement point, M, from the frame coordinates system is shown with vectors that include machine errors and nominal carriage motion. Setting the two paths to the measurement point equal we get Eqn. 1.

$$\vec{\mathrm{P}} + \vec{\mathrm{C}} + \vec{\mathrm{Z}} = \vec{\mathrm{X}} + \vec{\mathrm{B}} + \overrightarrow{\mathrm{Pr}} \qquad \textbf{Eqn. 1}$$

The part vector, $\vec{\mathrm{P}}$, and probe vector, $\overrightarrow{\mathrm{Pr}}$, terminate at the measurement point. The vectors can be represented in the coordinate system in which they are supported and measured as shown in Eqn. 2 to Eqn. 7. Here the vector $\vec{\mathrm{P}}$ in the c coordinate system is written $[\vec{\mathrm{P}}]_C$.

$$\vec{\mathrm{P}} = \overrightarrow{{}_{o}\mathrm{CM}} = [\vec{\mathrm{P}}]_C \qquad \textbf{Eqn. 2}$$

$$\overrightarrow{\mathrm{Pr}} = \overrightarrow{{}_{o}\mathrm{BM}} = [\overrightarrow{\mathrm{Pr}}]_B \qquad \textbf{Eqn. 3}$$

$$\vec{\mathrm{C}} = \overrightarrow{{}_{o}\mathrm{Z}{}_{o}\mathrm{C}} = [\vec{\mathrm{C}}]_Z \qquad \textbf{Eqn. 4}$$

$$\vec{\mathrm{Z}} = \overrightarrow{{}_{o}\mathrm{F}{}_{o}\mathrm{Z}} = [\vec{\mathrm{Z}}]_F \qquad \textbf{Eqn. 5}$$

$$\vec{\mathrm{X}} = \overrightarrow{{}_{o}\mathrm{F}{}_{o}\mathrm{X}} = [\vec{\mathrm{X}}]_F \qquad \textbf{Eqn. 6}$$

$$\vec{\mathrm{B}} = \overrightarrow{{}_{o}\mathrm{X}{}_{o}\mathrm{B}} = [\vec{\mathrm{B}}]_X \qquad \textbf{Eqn. 7}$$

The vectors represented in their supporting coordinate system can be transformed to a common representation to allow the addition in Eqn. 8.

$$[\vec{\mathrm{P}}]_F + [\vec{\mathrm{C}}]_F + [\vec{\mathrm{Z}}]_F = [\vec{\mathrm{X}}]_F + [\vec{\mathrm{B}}]_F + [\overrightarrow{\mathrm{Pr}}]_F \qquad \textbf{Eqn. 8}$$

Rotation transformations are needed to get the vectors represented in the same coordinate system shown in Eqn. 9 with the transformation from the c coordinate system to the frame coordinate system shown as $R_{\overline{CF}}$.

$$[\vec{\mathrm{P}}]_F = R_{\overline{CF}}[\vec{\mathrm{P}}]_C = R_{\overline{ZF}}R_{\overline{CZ}}[\vec{\mathrm{P}}]_C \qquad \textbf{Eqn. 9}$$

Since the transformation from the c coordinate system to the frame coordinate system isn't direct, it must first be transformed to the z coordinate system then to the frame coordinate system as shown in Eqn. 9. Similar methods are used below to transform the vectors to the frame coordinate system for addition.

$$[\vec{\mathrm{C}}]_F = R_{\overline{ZF}}[\vec{\mathrm{C}}]_Z \qquad \textbf{Eqn. 10}$$

$$[\vec{\mathrm{Z}}]_F = [\vec{\mathrm{Z}}]_F \; as\; measured \qquad \textbf{Eqn. 11}$$

$$[\vec{\mathrm{X}}]_F = [\vec{\mathrm{X}}]_F \; as\; measured \qquad \textbf{Eqn. 12}$$

$$[\vec{\mathrm{B}}]_F = R_{\overline{XF}}[\vec{\mathrm{B}}]_X \qquad \textbf{Eqn. 13}$$

$$[\overrightarrow{\mathrm{Pr}}]_F = R_{\overline{BF}}[\overrightarrow{\mathrm{Pr}}]_B = R_{\overline{XF}}R_{\overline{BX}}[\overrightarrow{\mathrm{Pr}}]_B \qquad \textbf{Eqn. 14}$$

By plugging Eqn. 9 to Eqn. 14 into Eqn. 8 we get Eqn. 15.

$$R_{\overline{ZF}}R_{\overline{CZ}}[\vec{\mathrm{P}}]_C + R_{\overline{ZF}}[\vec{\mathrm{C}}]_Z + [\vec{\mathrm{Z}}]_F = [\vec{\mathrm{X}}]_F + R_{\overline{XF}}[\vec{\mathrm{B}}]_X + R_{\overline{XF}}R_{\overline{BX}}[\overrightarrow{\mathrm{Pr}}]_B \qquad \textbf{Eqn. 15}$$

Solving for the part vector, in the c coordinate system gives Eqn. 16 where the probe vector is known from reading the displacement reading from the probe.

$$[\vec{\mathrm{P}}]_C = R_{\overline{CZ}}{}^{-1}\left[-[\vec{\mathrm{C}}]_Z + R_{\overline{ZF}}{}^{-1}\left[-[\vec{\mathrm{Z}}]_F + [\vec{\mathrm{X}}]_F + R_{\overline{XF}}\left[[\vec{\mathrm{B}}]_X + R_{\overline{BX}}[\overrightarrow{\mathrm{Pr}}]_B\right]\right]\right] \qquad \textbf{Eqn. 16}$$

3.4 Putting error motions into the model

The vectors and rotation transformation matrices include the nominal carriage movements and the 29 error motions described in Table 1. The squareness and parallelism terms are omitted.

$$\vec{\mathrm{P}} = \begin{bmatrix} X_P \\ Y_P \\ Z_P \end{bmatrix} \qquad \textbf{Eqn. 17}$$

$$\overrightarrow{\mathrm{Pr}} = \begin{bmatrix} X_{Pr} \\ Y_{Pr} \\ Z_{Pr} \end{bmatrix} \qquad \textbf{Eqn. 18}$$

$$\vec{\mathrm{C}} = \begin{bmatrix} \delta_x(\gamma) \\ \delta_y(\gamma) \\ \delta_z(\gamma) \end{bmatrix} \qquad \textbf{Eqn. 19}$$

$$\vec{\mathrm{Z}} = \begin{bmatrix} \delta_x(Z) \\ \delta_y(Z) \\ \mathrm{Z} + \delta_z(Z) \end{bmatrix} \qquad \textbf{Eqn. 20}$$

$$\vec{\mathrm{X}} = \begin{bmatrix} \mathrm{X} + \delta_x(X) \\ \delta_y(X) \\ \delta_z(X) \end{bmatrix} \qquad \textbf{Eqn. 21}$$

$$\vec{\mathrm{B}} = \begin{bmatrix} \delta_x(\beta) \\ \delta_y(\beta) \\ \delta_z(\beta) \end{bmatrix} \qquad \textbf{Eqn. 22}$$

Transformation matrices for the angular errors are shown in Eqn. 23 to Eqn. 26. Given the magnitude of the errors, the small angle approximation is used. The angular error transformation matrices equate to the multiplication of three rotation matrices, one for each angular error, with sine values replaced by their argument and cosine values by "1"[1].

$$R_{\overline{CZ}} = \begin{bmatrix} 1 & -\varepsilon_c(\gamma) & \varepsilon_b(\gamma) \\ \varepsilon_c(\gamma) & 1 & -\varepsilon_a(\gamma) \\ -\varepsilon_b(\gamma) & \varepsilon_a(\gamma) & 1 \end{bmatrix} \begin{bmatrix} \cos\gamma & -\sin\gamma & 0 \\ \sin\gamma & \cos\gamma & 0 \\ 0 & 0 & 1 \end{bmatrix} \qquad \textbf{Eqn. 23}$$

$$R_{\overline{ZF}} = \begin{bmatrix} 1 & -\varepsilon_c(Z) & \varepsilon_b(Z) \\ \varepsilon_c(Z) & 1 & -\varepsilon_a(Z) \\ -\varepsilon_b(Z) & \varepsilon_a(Z) & 1 \end{bmatrix} \qquad \textbf{Eqn. 24}$$

$$R_{\overline{XF}} = \begin{bmatrix} 1 & -\varepsilon_c(X) & \varepsilon_b(X) \\ \varepsilon_c(X) & 1 & -\varepsilon_a(X) \\ -\varepsilon_b(X) & \varepsilon_a(X) & 1 \end{bmatrix} \qquad \textbf{Eqn. 25}$$

$$R_{\overline{BX}} = \begin{bmatrix} 1 & -\varepsilon_c(\beta) & \varepsilon_b(\beta) \\ \varepsilon_c(\beta) & 1 & -\varepsilon_a(\beta) \\ -\varepsilon_b(\beta) & \varepsilon_a(\beta) & 1 \end{bmatrix} \begin{bmatrix} \cos\beta & 0 & \sin\beta \\ 0 & 1 & 0 \\ -\sin\beta & 0 & \cos\beta \end{bmatrix} \qquad \textbf{Eqn. 26}$$

Rotation transformation matrices for the nominal carriage positions are shown in Eqn. 23 and Eqn. 26 where the b

carriage rotates around the y axis and the c carriage rotates around the z axis. The order of the rotation matrix multiplication for nominal carriage positions and angular errors depends on how the errors are measured. The rotary carriage squareness and parallelism errors would be included in their infinitesimal rotation matrices. Linear stage squareness is added to the straightness.

4. Error compensation

The measurement points of a freeform optic are calculated using the machine positions and probe reading with the mathematical machine model which allows for the machine errors to be corrected. The mathematical model has inputs for the 29 machine errors (32-3, see Section 3.1 above) and probe errors as well as the uncertainty in the measurement of those errors. The systematic errors can be corrected while the stochastic errors will be accounted for in the uncertainty distributions used in the Monte Carlo simulation.

5. Monte Carlo simulation

The Monte Carlo simulation is a method of 'randomly' sampling from a number of different probability distributions to obtain numerical results. This is done many times with each iteration representing a possible 'true' value. The probability distributions are used to define the uncertainty in the machine error measurements, thermal effects, and probe errors.

A way to think about this method is to imagine that each iteration of the Monte Carlo simulation is a possible machine [4]. The part measured by each "machine" will have slight variations due to the uncertainty in the error measurements, probe, etc. The Monte Carlo simulation uses the mathematical model discussed above. For an iteration, each error is found by sampling from the uncertainty probability distribution, associated with that error, added to the nominal error value for the machine position. Each iteration will produce a set of points. The measurand (prescription) is fit to the set of points and subtracted. For, n, iterations of the Monte Carlo, there will be a set of deviations from the prescription that can be described by a probability distribution function, parameters or a visual representation.

5.1 Task specific uncertainty

The uncertainty of a measurement result is found using the Monte Carlo simulation with the mathematical machine model and the uncertainty for the machine error measurements, probe reading, and thermal effects. The two types of uncertainty categories outlined in the GUM will be considered, with type A being of statistical evaluation of experimental data while type B is other methods (see description in [4]). Using the Monte Carlo simulation it is possible to obtain a task specific uncertainty for the surface measured determining the most probable surface and the evaluated uncertainty.

6. Measuring the 3 mirror anastigmatic telescope optics

Three sets of the freeform mirrors will be manufactured, two with nickel coated aluminum and one from silicon carbide. The first set of nickel coated aluminium optics, one will be scaled down by half and used to demonstrate metrology techniques for wavefront testing. Measurements from the 100UMM can be input into optical design software to estimate a wavefront to compare with the measured wavefront.

Non-contact probes will be used to measure the optics with sampling or measuring strategies that reduce the thermal effects in measurement while providing dense enough data for measuring form. The 100UMM will be used for acceptance testing of the optics while a Mahr MarSurf LD 260 profilometer fitted with an additional linear stage and rotary stage will be used for in process metrology. The shape of the optics will converge toward the prescription and the errors in the profilometer. Using the 100UMM for acceptance testing provides an independent test unlikely to have the same uncorrected bias (if any) of the profilometer.

7. Metrology "probe path" generation

To generate the "probe path" for the measurement the nominal shape of the part, thermal effects, and data spacing are considered. The nominal surface is defined by either Zernike, Chebyshev or Forbes polynomials and input into MATLAB where, using the machine model, the machine carriage positions for a desired "probe path" are solved for and the g-code is generated.

By reading the scales and probe simultaneously it is possible to measure in a 'scanning' mode reducing the total measurement time and reducing thermal effects. Triggering the measurement using the machine code is also possible for a point by point measurement. Using 'scanning' mode, diametral or radial and outward spiral measurements are possible while for a point by point mode it is possible to do a cartesian grid, diametral or radial and a series of circumference measurements. A combination of these sampling strategies has been used to reduce thermal effects.

Point by point measurements reduce the data age uncertainty while taking more time to complete a measurement which could increase the thermal effects. The data density is also reduced compared to a 'scanning' mode unless the measurement time is increased significantly. For point by point, the machine has to stop at a measurement point and allow the machine to settle out before triggering. The 100UMM is set up to trigger a measurement in NI LabVIEW using m-code in the machine programming language.

Data spacing is selected to be of appropriate density for form measurements as the mid-spatial and roughness measurements will be completed on different instruments.

8. Conclusions

Measuring freeforms and evaluating the uncertainty is not a new problem. Freeform optics in the 250 mm class offer a set of challenges which solution will incorporate a mix of traditional and new metrology techniques and instruments. The procedure outlined here is a proposed approach to reducing and quantifying the measurement uncertainty.

Once manufactured, the three sets of optics from the 3 mirror anastigmatic telescope will be measured and the wavefront testing of the half scale optics will be completed. Multiple measurement strategies will be compared and the thermal effects characterized.

References

[1] R. J. Hocken and P. H. Pereira, Coordinate Measuring Machines and Systems, Boca Raton: CRC Press, 2012.

[2] G. Zhang et al, A Displacement Method for Machine Geometry Calibration, National Bureau of Standards – USA, 1988.

[3] ISO 230-1, Test code for machine tools – Part 1: Geometric accuracy of machine operating under no-load or quasi-static conditions, 2012.

[4] R.G. Wilhelm, R. Hocken, and H. Schwenke, 2001, Task Specific Uncertainty in Coordinate Measurement, *CIRP Annals*, **50** 553-563

[5] K. Rost, K. Wendt, and F. Hartig, 2016, Evaluating a task-specific measurement uncertainty for gear measuring instruments via Monte Carlo Simulation, *Precision Engineering,* **44** 220-230